

Insights into the unfolding pathway and identification of thermally sensitive regions of phytase from *Aspergillus niger* by molecular dynamics simulations

Kapil Kumar¹ · Krunal Patel² · D C Agrawal^{2,3} · J M Khire¹

Received: 12 December 2014 / Accepted: 4 May 2015 / Published online: 4 June 2015
© Springer-Verlag Berlin Heidelberg 2015

Abstract Thermal stability is of great importance in the application of commercial phytases. Phytase A (PhyA) is a monomeric protein comprising twelve α -helices and ten β -sheets. Comparative molecular dynamics (MD) simulations (at 310, 350, 400, and 500 K) revealed that the thermal stability of PhyA from *Aspergillus niger* (*A. niger*) is associated with its conformational rigidity. The most thermally sensitive regions were identified as loops 8 (residues 83–106), 10 (161–174), 14 (224–230), 17 (306–331), and 24 (442–444), which are present on the surface of the protein. It was observed that solvent-exposed loops denature before or show higher flexibility than buried residues. We observed that PhyA begins to unfold at loops 8 and 14, which further extends to loop 24 at the C-terminus. The intense movement of loop 8 causes the helix H2 and beta-sheet B3 to fluctuate at high temperature. The high flexibility of the H2, H10, and H12 helices at high temperature resulted in complete denaturation. The high mobility of loop 14 easily transfers to the adjacent helices H7, H8, and H9, which fluctuate and partially unfold at high

temperature (500 K). It was also observed that the salt bridges Asp110–Lys149, Asp205–Lys277, Asp335–Arg136, Asp416–Arg420, and Glu387–Arg400 are important influences on the structural stability but not the thermostability, as the lengths of these salt bridges did not increase with rising temperature. The salt bridges Glu125–Arg163, Asp299–Arg136, Asp266–Arg219, Asp339–Lys278, Asp335–Arg136, and Asp424–Arg428 are all important for thermostability, as the lengths of these bridges increased dramatically with increasing temperature. Here, for the first time, we have computationally identified the thermolabile regions of PhyA, and this information could be used to engineer novel thermostable phytases. Numerous homologous phytases of fungal as well as bacterial origin are known, and these homologs show high sequence similarity. Our findings could prove useful in attempts to increase the thermostability of homologous phytases via protein engineering.

Keywords Phytase A · Thermostability · Molecular dynamics simulations · Conformational dynamics · Structurally weak regions

Kapil Kumar and Krunal Patel contributed equally to this work.

Electronic supplementary material The online version of this article (doi:10.1007/s00894-015-2696-z) contains supplementary material, which is available to authorized users.

✉ J M Khire
jm.khire@ncl.res.in

¹ NCIM, Biochemical Sciences Division, Dr. Homi Bhabha Road, Pune 411 008, India

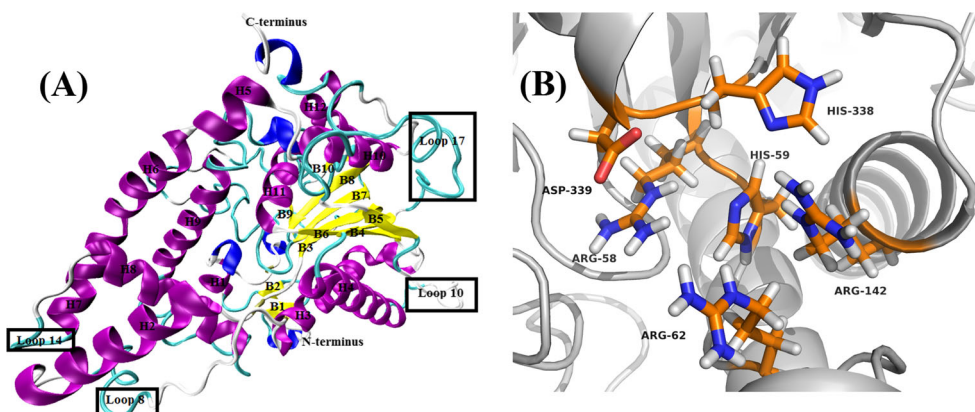
² Plant Tissue Culture Division, CSIR-National Chemical Laboratory, Dr. Homi Bhabha Road, Pune 411 008, India

³ Present address: Institute of Biochemical Sciences and Technology, Chaoyang University of Technology, 168 Jifeng E. Road, Wufeng, Taichung 41439, Taiwan

Introduction

Phytases are enzymes that hydrolyze phytic acid and phytate into inositol and phosphoric acid (or phosphate). They not only efficiently improve the utilization rate of phytate phosphorus in feed but also reduce environmental pollution from phytate phosphorus excreted by swine and poultry [1, 2]. *A. niger* phytase A (PhyA; Fig. 1a) consists of a large α/β -domain and a small α -domain [3]. The large α/β -domain contains a twisted six-stranded β -sheet with two long α -helices on one side and several short α -helices on the other. The small α -domain consists of a central long α -helix

Fig. 1a–b Structure of phytase A: **a** all α -helices, β -sheets, and important loops are labeled as *H*, *B*, and *Loop*; **b** catalytic residues are highlighted and labeled



surrounded by seven shorter α -helices. The labels and residue numbers of the α -helices, β -sheets, and loops in PhyA are listed in Table 1, while Fig. 1a depicts the structure of PhyA and the positions of some of the α -helices, β -sheets, and important loops within it. While the roles of hydrogen bonding, hydrophobic interactions, and C-terminal segments in the structural stability of many proteins have been studied [4–12], the specific roles of salt bridges and interactions between secondary structural elements in the thermostability of PhyA have not yet been explored in detail.

Native PhyA exhibits optimal activity at 50 °C and pH 5.0. As it is an acidic phytase, PhyA has been used in animal feed and food processing [3]. The catalytic core of PhyA comprises Arg58, His59, Arg62, Arg142, His338, and Asp339 (Fig. 1b). Any change in the conformations of catalytic residues or neighboring residues may lead to a loss of catalytic activity, as the distances between catalytic or binding residues influence this activity. Conformational changes to catalytic-site residues (or residues close to them) were found to occur when the simulation temperature was increased from 310 to 400 K, leading to a loss of enzymatic activity above 65 °C. It would therefore be very useful to increase the thermostability of phytases without affecting their catalytic efficiency, as this would extend their range of applications, enhance their effectiveness, and reduce their cost.

Identifying the regions or sites that are responsible for the thermal stability of PhyA may be useful for site-directed mutagenesis [13, 14]. A previous study showed that C-terminus deletion can greatly increase the thermal stability of a phytase (AppA in *E. coli*) [15]. The C-terminus has a destabilizing effect on the α/β fold in AppA, so deleting the C-terminus increased the thermostability of AppA by 39.07 %. In another study, the thermostability of AppA was enhanced by implementing mutations that enhanced several hydrogen bonds [16]. These mutations were introduced after comparing the structure of PhyA with a close homolog, the thermostable phytase in *Aspergillus fumigatus*, and then selecting useful hydrogen-bonding and ionic interactions by rational design. *Aspergillus fumigatus* phytase is the only phytase that refolds

efficiently after denaturation and retains 90 % of its initial activity after being heated at 100 °C for 20 min [17]. As Noorbatcha et al. have shown, the number of salt bridges does not have a significant influence on the stability of PhyA whereas the locations of the salt bridges do [18]. They compared the stabilities of two phytases with respect to the behavior of secondary structural elements and found that loops stabilize the phytase structure. In the same study, the authors performed a comparison of the root mean square deviations (RMSDs) of all loops, helices, and beta-sheets. Chen et al. also discussed the role of noncovalent intramolecular interactions in the thermostability of barnase [19]. Some experimental studies have reported that phytase thermostability was enhanced using various methods, including the introduction of a consensus sequence [20, 21], rational design [16, 22], directed evolution [23, 24], and the introduction of hydrogen bonds or ionic interactions [13, 17]. Using MD simulation, numerous sites and regions in many proteins have been recognized as enhancing thermal stability [17, 25–32]. Several factors that may influence protein thermal stability have also been identified through MD simulation, such as flexibility [31], hydrogen bonds [27], disulfide bonds [33], and salt bridges [34, 35]. Thus, many structural features contribute to the thermostability and folding of proteins, and there is no single factor that can explain the thermal adaptation of enzymes. Although considerable insight has been gained from theoretical and experimental studies of protein folding and thermostability, we still possess little knowledge of how enzymes have adapted during the course of evolution. Therefore, further studies are needed on thermostability and protein folding since they may provide valuable information on evolutionary aspects of the thermal stability of proteins. Moreover, they may aid in the design of more thermostable proteins that can function at high temperatures.

In the work reported in the present article, the conformational dynamics of PhyA were studied via MD simulations. MD simulation studies were used to analyze the changes in the global structural stability, dynamic features, and salt bridges of PhyA that occurred upon enhancing the simulated

Table 1 Structure designations of PhyA helices, β -sheets, and loops

α -Helices (H)	β -Sheets (B)	Loops (L)
19–23 H1, 66–82 H2,	9–10 B1, 14–15 B2,	7–8 L1, 11–13 L2, 16–18 L3,
107–129 H3, 141–160 H4,	48–58 B3, 134–139 B4,	24–25 L4, 29–34 L5, 38–47 L6,
193–197 H5, 199–210 H6,	175–178 B5, 332–337 B6,	59–65 L7, 83–106 L8, 130–133 L9,
212–223 H7, 231–247 H8,	383–391 B7, 398–403 B8,	161–174 L10, 179–192 L11,
264–280 H9, 293–305 H10,	406–407 B9, 420–421 B10	198–201 L12, 211–213 L13,
339–349 H11, 423–435 H12		224–230 L14, 248–263 L15,
		281–289 L16, 306–331 L17,
		338–341 L18, 350–382 L19,
		392–396 L20, 404–405 L21,
		408–420 L22, 436–438 L23,
		442–444 L24

temperature. The thermosensitive regions of PhyA were identified from its conformational dynamics. By calculating root mean square deviation (RMSD) and root mean square fluctuation (RMSF) values for backbone and C α atoms, the thermally sensitive regions of PhyA were identified. The dynamic properties of PhyA at different temperatures were compared in terms of secondary structure content, molecular flexibility, main chain to main chain hydrogen bonds, and salt-bridge interactions. Our analysis specifically focused on the identification of thermally sensitive regions, the sites at which unfolding was initiated, and the contribution of salt bridges to the stability of this protein.

Materials and methods

Protein preparation

The crystal structure of *A. niger* PhyA was obtained from the database of the Research Collaboratory for Structural Bioinformatics (RCSB) (PDB ID: 3K4Q). Some residues were missing from the crystal structure; these were modeled with the help of the Modeller software package using 3K4Q as the template [3]. A self-template was used because of the high sequence homology with the crystal structure [36].

Simulation methods

To investigate the structural consequences, PhyA was solvated using the TIP3P water model [37]. A dodecahedral box ($10.43 \times 10.43 \times 7.73 \text{ \AA}^3$) was selected to perform MD simulation. The total number of solvent molecules used was 24,269. The system was neutralized by adding counterions (65 sodium and 48 chloride ions). All MD simulations were performed under periodic boundary conditions using the GROMACS (version 5.0) software package [38] and the AMBER ff99SB force field [39]. Commonly used force-field

parameters are expected to be valid at ambient temperature, but numerous studies have shown that the same parameters can also be applied when working at very high temperatures and have offered a qualitative explanation for this phenomenon [40–46]. The energy of the system was minimized using the steepest descent algorithm for 5000 steps to remove any bad clashes generated by solvent molecules. An equilibration MD was run for 1 ns to completely mix and equilibrate the contents of the box. Complete mixing and equilibration of the contents were confirmed by the convergence of the potential energy and temperature of the system. All production MD simulations were performed within NPT (the number of atoms, pressure, and temperature were kept constant throughout the simulation) ensembles. The Nosé–Hoover and Parrinello–Rahman methods were utilized to control temperature and pressure, respectively [47, 48]. The LINCS algorithm was used to constrain all bond lengths and the SETTLE algorithm was used for water molecules [49, 50]. The particle mesh Ewald (PME) method was used to model non-bonded electrostatic and LJ interactions, as it is known to be the best method for computing long-range electrostatics [51]. 30-ns production MD simulations were performed at 310, 350, 400, and 500 K. In those simulations, the density of water was decreased as the temperature was increased due to vapor–liquid coexistence at 350, 400, and 500 K; see the “Electronic supplementary material” (ESM), Fig. S1.

Analysis

All of the analyses were performed using the analytical tools in GROMACS. VMD was used to visualize trajectories and produce structural diagrams [52]. The RMSF of PhyA from the MD trajectory at 310 K was also calculated and compared with the crystallographic B factor, another indicator of backbone flexibility. Global consistency was observed, which confirmed that the MD simulation of this system was reliable. Prior to calculating the fluctuations in atomic positions, we

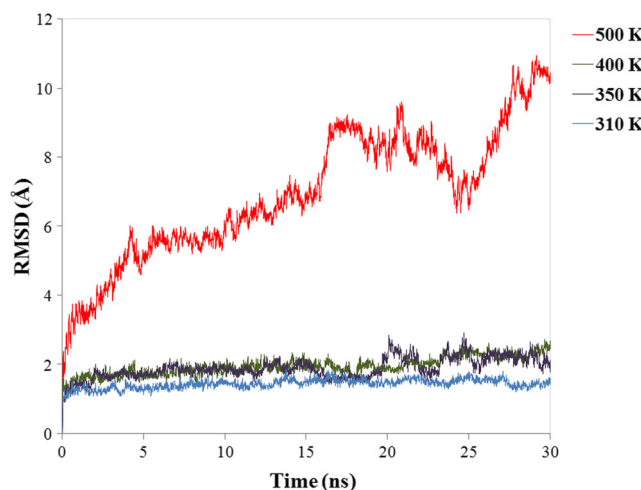


Fig. 2 Time evolution of the backbone RMSD versus the starting structure of PhyA. The simulation data obtained at 310, 350, 400, and 500 K are shown in blue, violet, green, and red, respectively

removed the overall translational and rotational motions by superimposing the C α atoms of each snapshot structure onto those of the starting structure of the trajectory using the least-squares fitting method. RMSD, RMSF, and DSSP [53] values were calculated to analyze structural stability and denaturation. In this study, a salt bridge was considered to be formed if the distance between an oxygen atom of an acidic residue and the nitrogen atom of a basic residue was less than 5 Å for at least 50 % of the simulation time. The average lengths of the

salt bridges that fulfilled the abovementioned criteria were calculated for the last 10 ns of simulation time.

Results and discussion

Overall structural stability

The backbone RMSD was calculated during each MD simulation so that the differences between two simulated trajectories could be gauged. The plot (Fig. 2) shows that the systems are equilibrated and thus suitable for observing the dynamics of PhyA. The backbone RMSD remains at ~1.25 Å at 310 K and ~2.0 Å at 350 and 400 K. This indicates that the structures are stable and that no significant conformational changes occurred during the simulations performed at those temperatures. The similarity of the backbone RMSD values in the simulations at 350 and 400 K also indicates that these two MD trajectories are very similar. However, in the simulation at 500 K, the backbone RMSD increases rapidly and major structural distortion occurs. Thus, the three-dimensional structure of PhyA is denatured at 500 K.

The RMSF values increase drastically at 500 K. Some of the thermosensitive regions show significant fluctuations at 350 and 400 K (Fig. 3a). The radius of gyration does not show much fluctuation from the native state across the whole

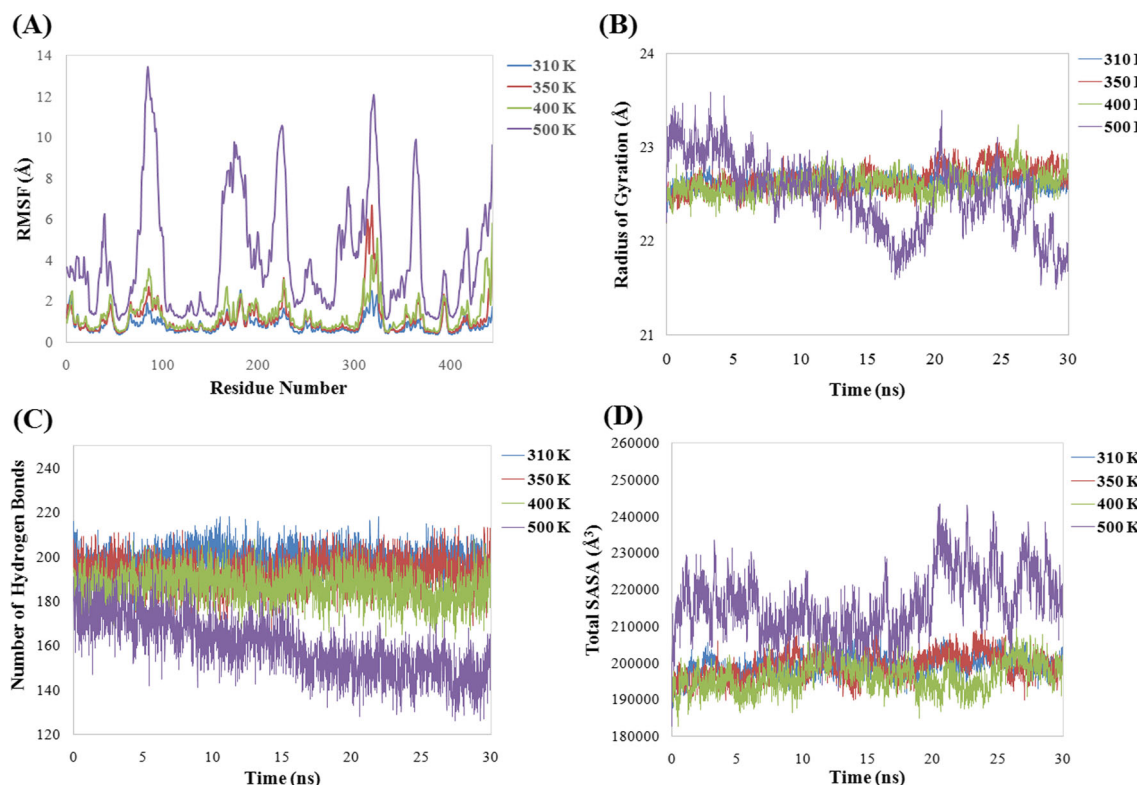


Fig. 3 **a** Residue RMSF; **b** radius of gyration (R_g); **c** number of main chain to main chain hydrogen bonds; **d** total solvent-accessible surface area (SASA). The simulation data obtained at 310, 350, 400, and 500 K are shown in blue, red, green, and violet, respectively

temperature range (Fig. 3b). High fluctuation of the backbone atoms at 500 K causes PhyA to enter a partially folded state. Fluctuations in the backbone atoms were observed at 500 K, probably due to a decrease in the number of main chain to main chain hydrogen bonds (Fig. 3c) which contribute greatly to the formation and stability of secondary structures. As the temperature is increased from 310 K to 400 K, the total number of main chain to main chain hydrogen bonds gradually decreases, implying that hydrogen bonding is an important factor in the thermostability of PhyA [12–19]. Also, the solvent-accessible surface area increases significantly at 500 K due to the unfolding of PhyA (Fig. 3d).

Dynamic features

The average RMSF values in an MD simulation are usually considered to be a good indicator of the overall flexibility of a protein. Thus, the RMSF values for the C α atoms with respect to each residue were calculated for each MD simulation at a different temperature. Figure 4a shows that the RMSF values of most regions of PhyA fluctuate only slightly at temperatures of up to 350 K, indicating that these regions are relatively thermostable. In contrast, some regions exhibited steep RMSF fluctuations at higher temperatures such as 350 and 400 K, indicating that these are thermally hypersensitive regions.

Likewise, using the average RMSF values of the secondary-structure residues (Fig. 4a and b), regions of PhyA with high flexibility can be identified and further insight into

the dynamics of PhyA can be obtained. Loops 8, 10, 14, 17, and 24 as well as B5, H2, H7, and H12 showed the highest average RMSF values. During the simulation at 310 K, H2 showed large fluctuations compared to those of neighboring loops (Fig. 4b). This high flexibility of H2 may be related to the activity of PhyA because all phytases are reported to show optimal activity levels at temperatures of around 50–55 °C. Large fluctuations of this helix might help to release the product, while large fluctuations in H7 are due to a loss of interaction between loop 14 and H2. The same idea applies for H10 and H12: both helices interact with each other at lower temperature, but these interactions do not exist at 350 and 400 K.

All of the β -strands have low average RMSF values compared to the helices and loops. The high rigidity of β -strands plays a very important role in thermostability. Optimal packing of the central β -strand is crucial to the formation of stable α/β -domain folding in PhyA. Figure 4b also shows that the β -strands are very stable, even under high thermal stress, although B5 showed higher fluctuations than all the other sheets.

Drastic increases in the RMSF values of loops 8, 10, 14, 17, and 24 upon shifting from low to high temperature indicates the need for these loops in order to thermostabilize PhyA (Fig. 4b). We can confirm that loops are essential for phytase thermostability because these loops show low RMSF values at low temperatures whereas these fluctuations increase drastically at 350 and 400 K. The greatest fluctuations were

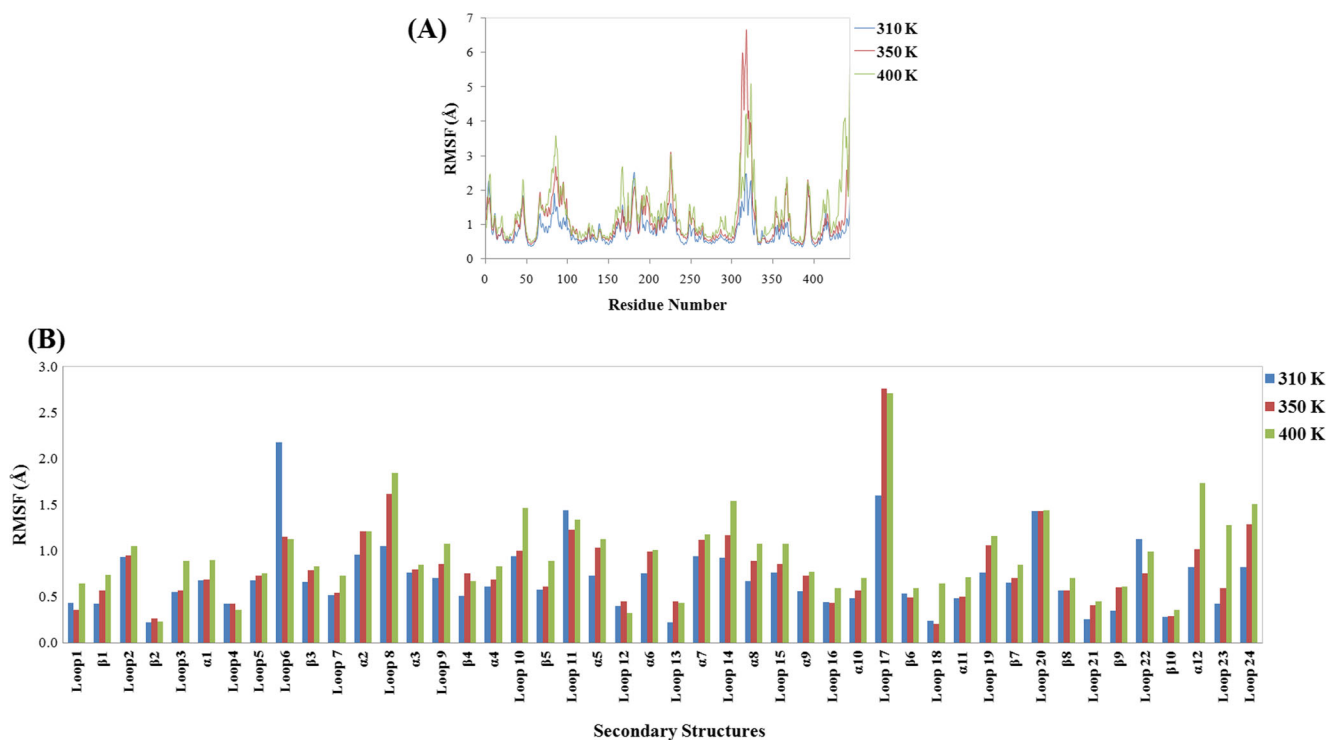


Fig. 4 **a** Residue RMSF; **b** average RMSF values of secondary structures. The simulation data obtained at 310, 350, and 400 K are shown in blue, red, and green, respectively

observed in loops 8, 10, 14, and 17. The largest increases in the fluctuations of loops 8 and 14 are due to the loss of an interaction between loop 12 and H2. The interaction between loop 10 and H3 is also lost and the rigidity of this loop decreases considerably at 350 and 400 K. Loop 17 stops interacting with loop 24 and the C-terminus at 350 and 400 K, and the C-terminus and loop 17 become very flexible. All four of these loops are located on the surface of PhyA, meaning that they are exposed to solvent and connected to secondary structures via weak interactions or they do not interact with them at all. The average RMSF values of the C-terminus are higher than those of the N-terminus [3]. The helix in the C-terminus is more flexible than the coil of the N-terminus (Fig. 4a). Thus, the C-terminus is less stable than the N-terminus at both low and high temperatures. The main reason for this could be the loss of interactions between loop 17 and 24 and H12 at 350 and 400 K, causing the C-terminus to fluctuate dramatically. Loop 17 is also solvent-exposed and interacts with H6; the loss of this interaction at 350 and 400 K causes conformational changes in the loop itself as well as nearby residues [54]. The conformational rigidity of the helices and β -sheets holds the native structure intact at 350 and 400 K. The loops are the regions that fluctuate the most at these temperatures, so strengthening the loops might help to enhance the thermostability of PhyA.

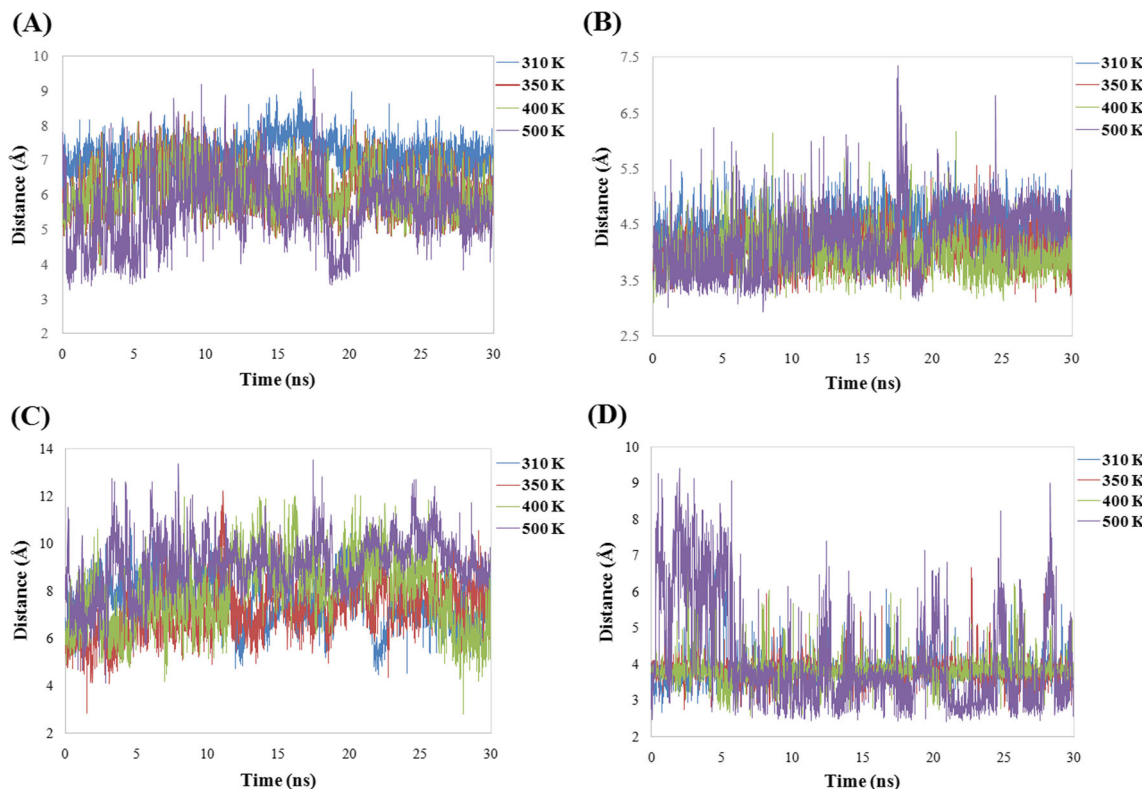


Fig. 5a–d Distances between oxygen and nitrogen atoms of catalytic-site residues: **a** Asp339–His59; **b** Asp338–Arg58; **c** Asp339–Arg62; **d** Asp339–Lys278. The simulation data obtained at 310, 350, 400, and 500 K are shown in blue, red, green, and violet, respectively

Changes in the conformations of catalytic residues

It was observed during experiments that PhyA starts to lose its activity at around 60 °C [1–3]. We measured the distances between catalytically important residues. The distance between the Asp339 oxygen and His59 nitrogen atoms decreases as the temperature is increased from 310 to 400 K, leading to greater rigidity of the catalytic site residues, which may be responsible for the loss of enzymatic function. Because phytate is a large molecule and has six doubly charged phosphate groups, electrostatic interactions between phytate and positively charged residues play a bigger role than other interactions. As high flexibility or large fluctuations is/are essential for the removal of a phosphate group, this process slows down at higher temperature due to enhanced rigidity of the flexible and large arginine side chains, resulting in loss of enzyme function. As the length Asp339–His59 (Fig. 5a) decreases slightly and the length Asp339–Arg58 (Fig. 5b) increases slightly, it is quite probable that a phosphate entity will not fit into the space between these residues. The lengths of other salt bridges such as Asp339–Arg62 (Fig. 6c) and Asp339–Lys278 (Fig. 5d) increase with increasing temperature in this temperature range. These slight changes in the distances between catalytic residues may be responsible for the loss of enzyme function. Also, the fluctuations of catalytic site residues (Fig. 6) confirmed that the volume of the catalytic pocket decreases slightly.

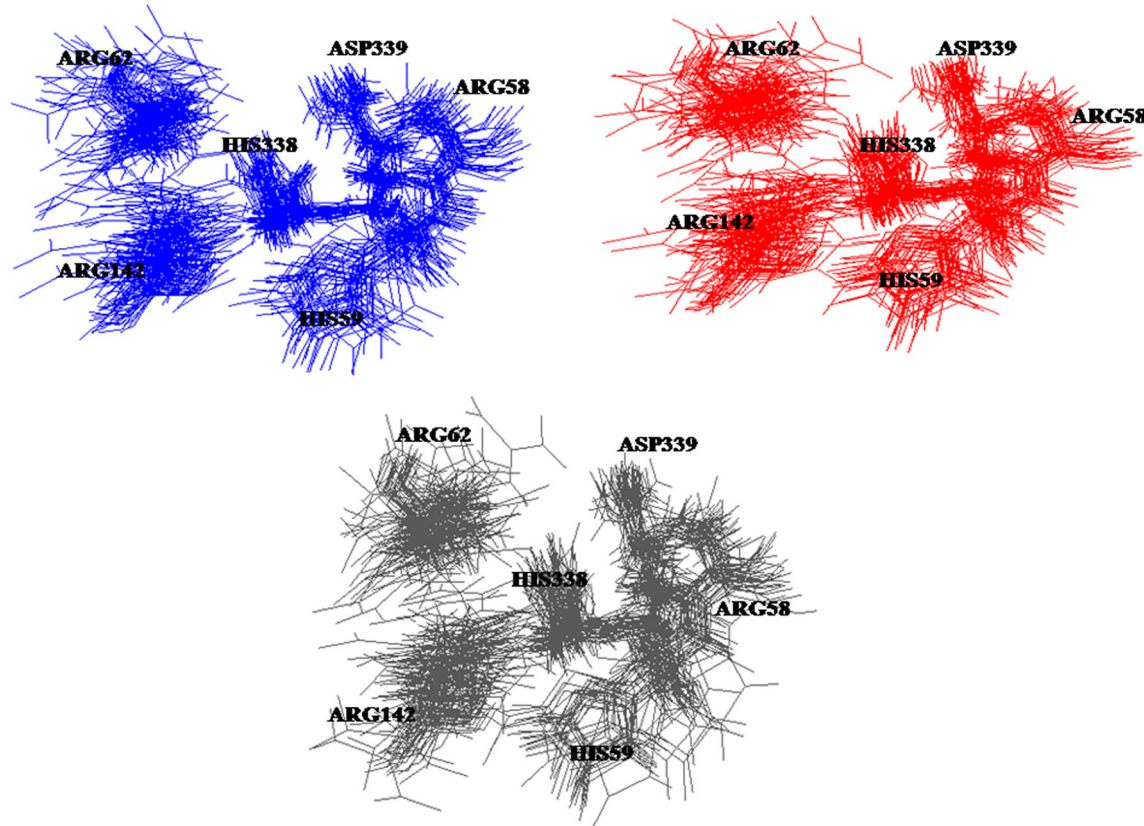


Fig. 6a–c Overall fluctuations of catalytic site residues during the whole simulation obtained at **a** 310 K, **b** 350 K, **c** 400 K (shown in blue, red, and gray, respectively)

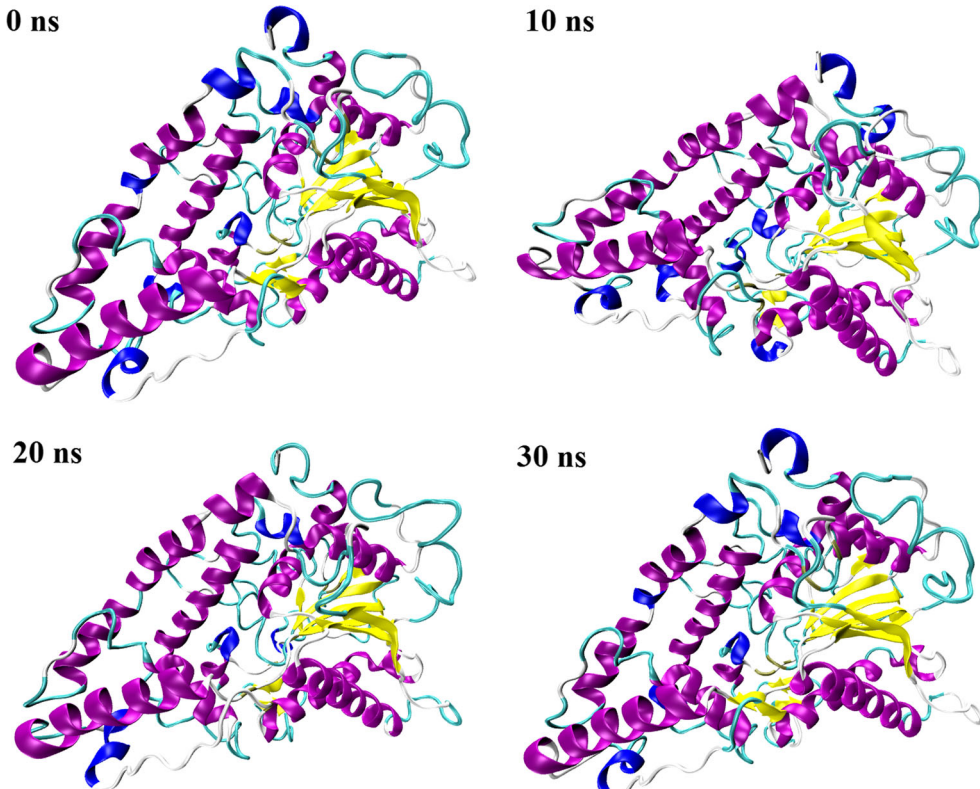
Conformational changes during high-temperature simulation

The unfolding of PhyA is shown in Figs. 7, 8, 9, and 10 as snapshots. Up to 400 K, PhyA does not start to unfold. As inferred from the RMSD and RMSF results, unfolding starts at 500 K within the first few nanoseconds of simulation. Herein, we describe in detail the structural changes that occur in different regions of phytase. Unfolding can happen when α -helices are gradually lost, starting from the N-terminus, and these structural changes can proceed towards the α -domain and α/β -domain. The α/β -domain is a stable region that is made up of several β -strands and α -helices, including B1–B10 and H1–H12, which are connected through loops. The six twisted β -strands form a central part of the hydrophobic core of the α/β -domain. Consequently, the loss of this structure is vital to the unfolding of HAP phytases.

Figure 11 shows changes in the secondary structure with simulation time that indicate the unfolding of PhyA at 500 K. At low temperatures up to 400 K, unfolding does not occur. As the temperature increases, the secondary structures in these areas show significant instability. Conformational fluctuations were observed consistently in those areas as the simulation time progressed. H5, H6, H7, and H12 are denatured completely during the simulation at 500 K (Figs. 10 and 11).

H2 and H10 are also denatured completely except for two or three residues that remain in a helical conformation. The most stable helices are H3, H4, H8, H9, and H11; these helices are partially denatured at 500 K. H3 and H4 are strongly connected via some salt bridges, increasing the stability of both helices. H8 and H9 are buried in the core of the α -domain, indicating resistance to denaturation. H11 is present at the interface between the α -domain and the α/β -domain, and the most protected region of PhyA contains a catalytic HD motif connected to other residues via salt bridges and hydrogen bonds. Throughout the simulations performed at 310–500 K, all β -strands are perfectly conserved except for B5, which denatures completely at 500 K. B5 is exposed to solvent, so it is obvious that this will be the first strand to denature. This fact further indicates that the stability of B5 and H5 depend on the stability of loop 10. The large fluctuations in loop 11 force B5 and H5 to adopt different conformations, leading to complete denaturation. The loops are the most thermosensitive structures of PhyA, especially loops 8, 10, 14, and 17. It has been reported that loop length affects protein thermostability [54]. The high mobility of the long loop 10 is easily transferred to the adjacent H5, H6, H7, and B5, causing them to fluctuate and leading to complete denaturation at high temperature. Thus, a stabilizing mutation, deletion, or shortening of this loop could be a promising way to improve thermostability.

Fig. 7 Snapshots (0, 10, 20, and 30 ns) of PhyA simulation at 310 K. β_{10} helices in blue, α -helices in purple, β -sheets in yellow, turns in cyan, coils in white



Loop 14 contains four amino acids and resides in the middle of the α -domain. Loop 8 resides in the vicinity of loop 14 and H2, so loops 8 and 14 can be connected by introducing a salt bridge or a disulfide bond, thus stabilizing H7, H8, H9, and H2. Regarding the termini, the direction of the N-terminus in the three-dimensional structure changes slightly whereas the

direction of the C-terminus changes dramatically during the MD simulations. The helix was found to be very well conserved in the C-terminus until the simulated temperature rose to 500 K. In general, for most of the proteins, the N-terminus shows more flexibility than the C-terminus. Hence, it can be inferred from our results that either stabilizing or deleting the

Fig. 8 Snapshots (0, 10, 20, and 30 ns) of PhyA simulation at 350 K. β_{10} helices in blue, α -helices in purple, β -sheets in yellow, turns in cyan, coils in white

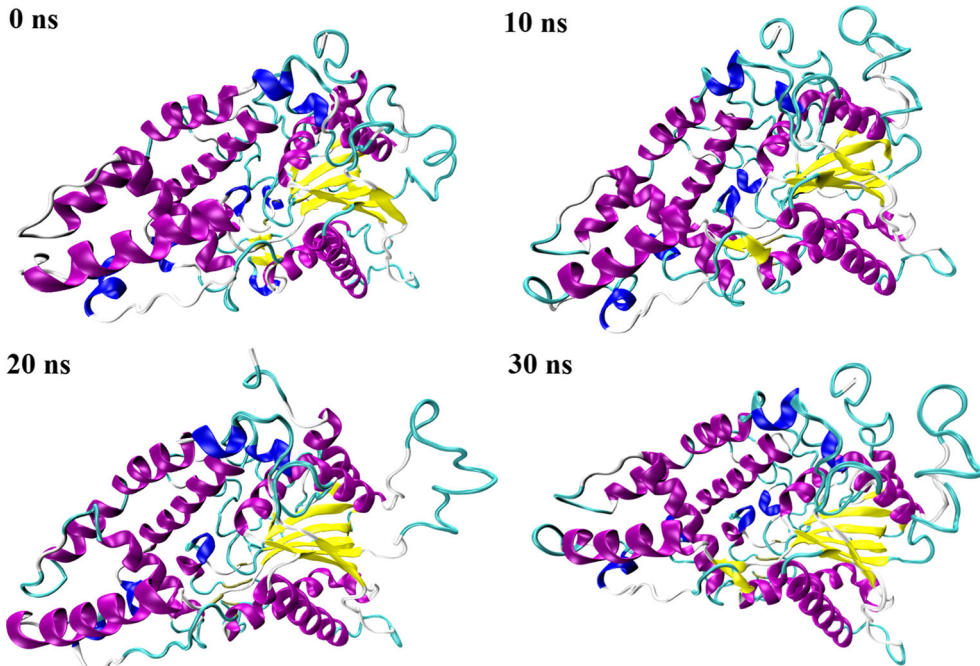
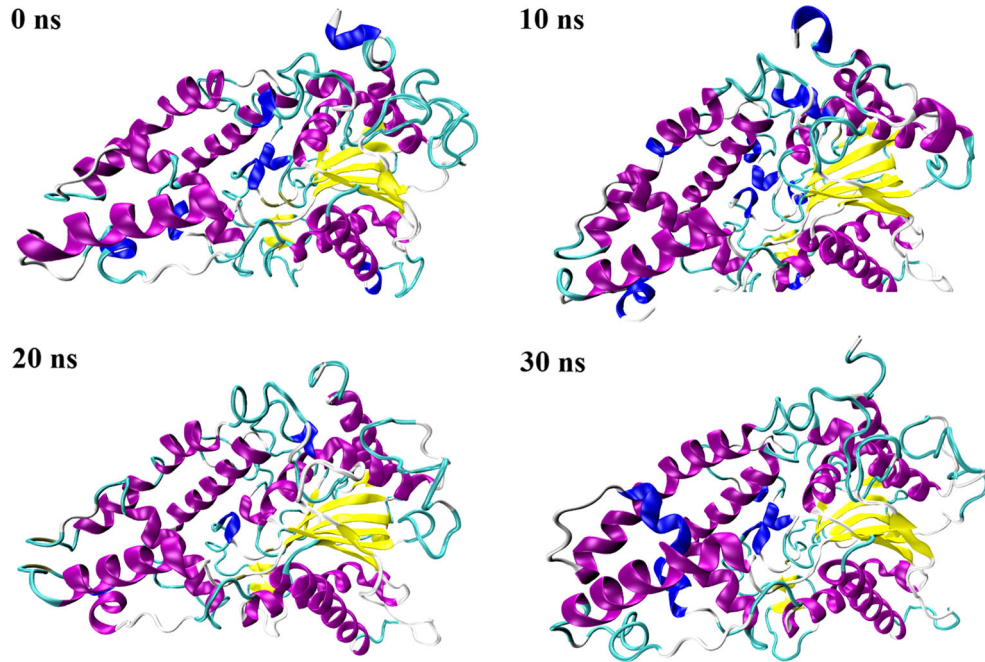


Fig. 9 Snapshots (0, 10, 20, and 30 ns) of PhyA simulation at 400 K. β_{10} helices in blue, α -helices in purple, β -sheets in yellow, turns in cyan, coils in white



C-terminus could result in a thermostable variant [15]. The results obtained in this study are qualitative rather than quantitative. However, simulation results can indicate the key amino acid residues responsible for thermostability and the target residues that should be submitted to site-directed mutagenesis

to enhance stability. Moreover, the simulation results described here are pretty consistent across the whole range of simulation temperatures and provide a good idea of the thermosensitive regions of PhyA and the initiation of its unfolding pathway.

Fig. 10 Snapshots (0, 10, 20, and 30 ns) of PhyA simulation at 500 K. β_{10} helices in blue, α -helices in purple, β -sheets in yellow, turns in cyan, coils in white

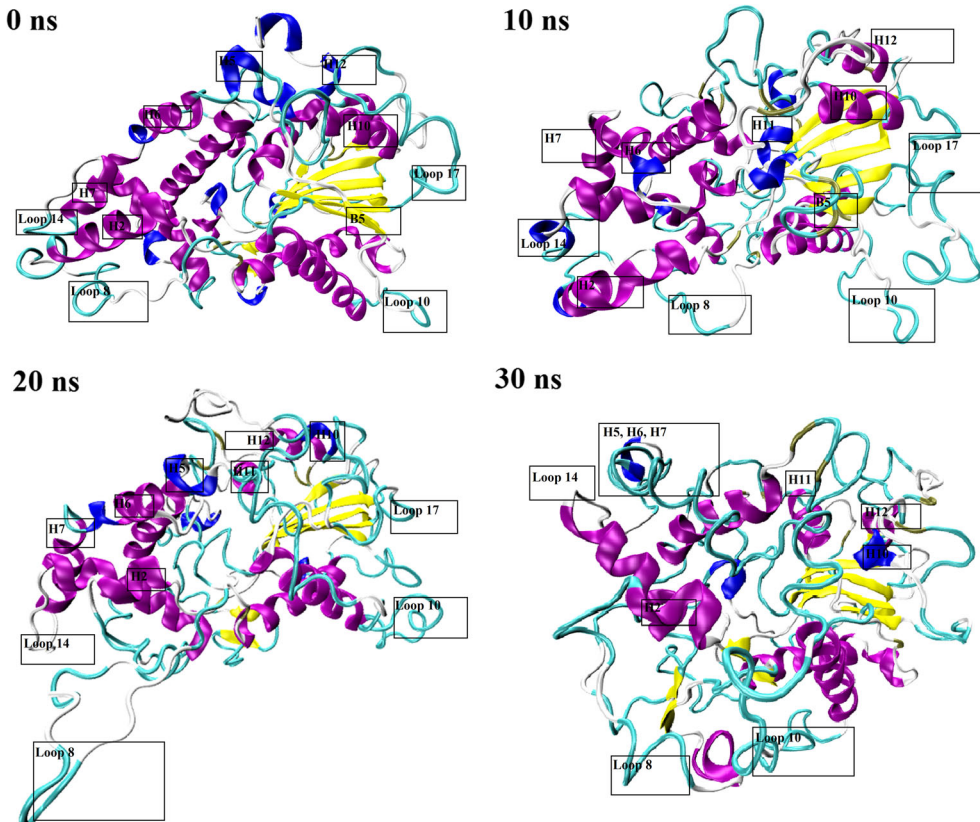
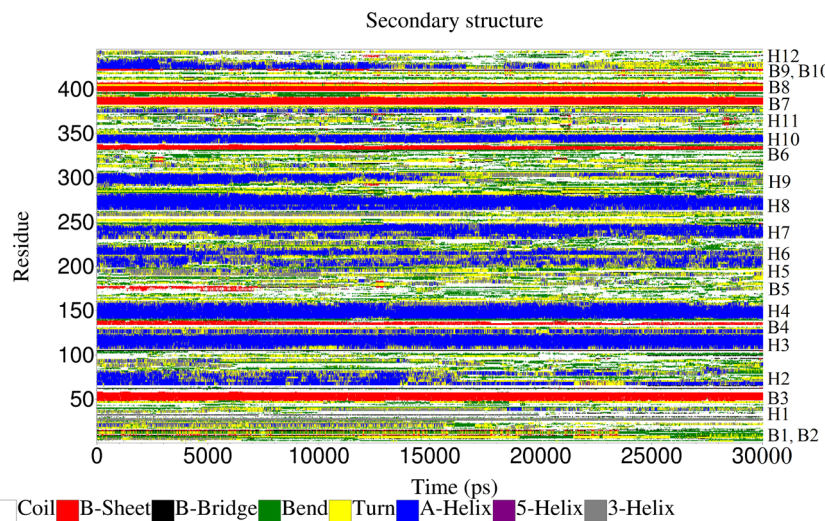


Fig. 11 High-temperature (500 K) denaturation of secondary structures of PhyA at different time points. Secondary structural elements by color: white coil, red β -sheets, black β -bridge, green bend, yellow turn, blue α -helix



Salt-bridge interaction analysis

The distances between the charged residues that form salt bridges in the crystal structure of PhyA during the simulations at 310, 350, 400, and 500 K were monitored and averaged. The salt bridges were identified using a 5-Å distance cutoff, and were only considered if they existed for more than 50 % of the simulation time. The length of each salt bridge was averaged over the last 10 ns of simulation time (Table 2). The salt bridges were divided into two categories: (1) salt bridges with lengths that

remain unaffected when the temperature is increased; (2) salt bridges with lengths that increase when the temperature is increased (Table 2) [9]. Analyzing the first category of salt bridges, we found crosslinking of Asp110–Lys149 with H3 and H4, Asp205–Lys277 with H6 and H9, and Glu387–Arg400 with B7 and B8. The lengths of these salt bridges remained constant at all temperatures, and these salt bridges were essential for structural stability but not for thermostability (Table 2). Other salt bridges between loops and secondary structures, such as the crosslinking of Asp335–Arg136 with B7 and loop 7 as well as Asp416–Arg420 with B10 and loop 23, were also not affected by increases in temperature. Those two salt bridges also helped to maintain the structural integrity of PhyA. Thus, these conserved salt bridges are very important as they help to keep the α/β fold stable, but they are only correlated with the structural stability of PhyA, not its thermostability. Noting the conformational changes that occur to the entire structure with increasing temperature and the locations of the salt bridges in Table 2, we can see that these salt bridges stabilize the region including H3, H4, H6, H9, B7, and B8. Asp335–Arg303 is a buried salt bridge located between B7 and H10. The length of this salt bridge increases dramatically during the last 10 ns of simulation at 500 K (Table 2). B7 is buried in the core of the α/β -domain, so the loss of this salt-bridge interaction could lead to the unfolding of the nucleus of PhyA. Similarly, the lengths of Asp424–Arg428, Asp266–Lys219, Asp339–Lys278, Glu125–Arg163, and Asp299–Arg136 change dramatically when the simulation temperature is increased (Table 2). These salt bridges are very sensitive to temperature changes and they influence the thermostability of PhyA. Thus, salt bridges are a major factor in protein thermostability. We also calculated the total

Table 2 Average lengths of salt bridges during the last 10 ns of simulation at 310, 350, 400, and 500 K

Salt bridge	310 K	350 K	400 K	500 K
Salt bridges with lengths that remain unaffected or increase only slightly with increasing temperature				
Glu110–Lys149	4.72	4.72	4.63	4.09
Glu205–Arg277	3.34	3.34	3.54	3.84
Glu387–Arg400	4.20	4.20	4.18	4.38
Asp335–Arg136	4.13	4.13	3.94	3.93
Asp416–Arg420	3.62	3.62	3.81	4.21
Salt bridges with lengths that increase significantly with increasing temperature				
Glu299–Arg136	3.46	3.46	3.38	7.52
Glu266–Arg219	3.53	3.53	3.50	6.13
Glu125–Arg163	5.48	7.82	8.48	13.21
Glu424–Arg428	5.48	4.99	6.71	8.67
Asp335–Arg303	3.47	3.47	3.87	8.01
Asp405–Lys119	4.33	4.33	6.32	4.45

number of salt bridges, which is highly temperature dependent. This confirms that it is not the presence of a salt bridge per se that strongly affects the overall thermostability of PhyA; the location of the salt bridge has a much greater impact [18]. Given the relatively high sequence similarity among all of the homologous phytases, it is reasonable to infer that all of these fungal phytases have conserved salt bridges. Similar findings have been observed for other fungal and bacterial phytases. *A. fumigatus* phytase is known for its high thermostability due to the presence of multiple salt bridges at specific locations. It possesses only 66 % sequence homology with PhyA, although their crystal structures are closely related. These salt bridges could be strengthened as a way to increase the thermostability of PhyA and other homologous phytases.

Conclusions

Based on RMSF calculations for PhyA at various temperatures, several thermally sensitive regions of PhyA were identified, such as H2, H12, loops 8, 10, 14, and 17, and the C-terminal end. Loops 8, 10, 14, and 17 have been shown to be the most thermosensitive of all. H5, H6, and H7 were affected by fluctuations of loop 10 and were found to be completely denatured within the first few nanoseconds of simulation at 500 K, while H2 and H10 remained partially folded. H12 was denatured completely, which affected the stability of the C-terminus as well as the whole protein. H3, H4, H8, H9, and H11 remained quite stable throughout the simulation at 500 K. Among all the β -sheets, only B5 was denatured completely during the 500 K simulation. The conformational rigidity of helices and β -sheets holds the native structure together at 350 and 400 K. The loops are the regions that fluctuate the most at these temperatures. Strengthening the loops may help to enhance the thermostability of PhyA. The total number of main chain to main chain hydrogen bonds gradually decreased when the temperature was raised from 310 to 500 K, indicating the importance of hydrogen bonds to the thermostability of PhyA [4]. Comprehensive analyses of salt-bridge interactions within structurally stable and thermally sensitive regions showed that, on the one hand, the formation of salt bridges can significantly improve the thermal stability of enzymes, and on the other, most salt bridges in the thermally sensitive regions are not strong enough to hold adjacent structures together and stop them from dissolving into the solvent. We also calculated the total number of salt bridges that are greatly affected at all temperatures, which confirmed that the presence of a salt bridge does not affect the overall thermostability of PhyA; the location of the salt bridge has a greater impact [18]. Considering the relatively high sequence similarity among the homologous phytases, it is reasonable to infer that all of the

fungal phytases have a similar heat-denaturing pathway. Therefore, according to the present simulation study, introducing one or more stable salt bridges into these thermally sensitive regions of industrialized phytases by clamping the bridges to nearby structural elements would be a promising way to markedly increase the thermal stability of these phytases.

Acknowledgments We acknowledge the Centre of Excellence in Advanced Computing, National Chemical Laboratory, Pune, for providing computational facilities. K. Kumar acknowledges the University Grant Commission and K. Patel acknowledges the Council of Scientific and Industrial Research for senior research fellowships.

References

1. Haefner S, Knietsch A, Scholten E, Braun J, Lohscheidt M, Zelder O (2005) Biotechnological production and applications of phytases. *Appl Microbiol Biotechnol* 68(5):588–597. doi:[10.1007/s00253-005-0005-y](https://doi.org/10.1007/s00253-005-0005-y)
2. Selle PH, Cowieson AJ, Ravindran V (2009) Consequences of calcium interactions with phytate and phytase for poultry and pigs. *Livest Sci* 124(1–3):126–141. doi:[10.1016/j.livsci.2009.01.006](https://doi.org/10.1016/j.livsci.2009.01.006)
3. Oakley AJ (2010) The structure of *Aspergillus niger* phytase PhyA in complex with a phytate mimetic. *Biochem Biophys Res Commun* 397(4):745–749. doi:[10.1016/j.bbrc.2010.06.024](https://doi.org/10.1016/j.bbrc.2010.06.024)
4. Eijsink VG, Bjork A, Gasicides S, Sirevag R, Synstad B, van den Burg B, Vriend G (2004) Rational engineering of enzyme stability. *J Biotechnol* 113(1–3):105–120. doi:[10.1016/j.jbiotec.2004.03.026](https://doi.org/10.1016/j.jbiotec.2004.03.026)
5. Kumar S, Tsai CJ, Nussinov R (2000) Factors enhancing protein thermostability. *Protein Eng Des Sel* 13(3):179–191
6. Pack SP, Yoo YJ (2003) Protein thermostability: structure-based difference of residual properties between thermophilic and mesophilic proteins. *J Mol Catal B Enzym* 26(3–6):257–264. doi:[10.1016/j.molcatb.2003.07.004](https://doi.org/10.1016/j.molcatb.2003.07.004)
7. Querol E, Perez-Pons JA, Mozo-Villarias A (1996) Analysis of protein conformational characteristics related to thermostability. *Protein Eng Des Sel* 9(3):265–271
8. Ragone R (2001) Hydrogen-bonding classes in proteins and their contribution to the unfolding reaction. *Protein Sci* 10(10):2075–2082. doi:[10.1110/ps.09201](https://doi.org/10.1110/ps.09201)
9. Szilagyi A, Zavodszky P (2000) Structural differences between mesophilic, moderately thermophilic and extremely thermophilic protein subunits: results of a comprehensive survey. *Structure* 8(5):493–504
10. Vieille C, Gregory Zeikus J (1996) Thermozyymes: Identifying molecular determinants of protein structural and functional stability. *Trends Biotechnol* 14(6):183–190. doi:[10.1016/0167-7799\(96\)10026-3](https://doi.org/10.1016/0167-7799(96)10026-3)
11. Vieille C, Zeikus GJ (2001) Hyperthermophilic enzymes: sources, uses, and molecular mechanisms for thermostability. *Microbiol Mol Biol Rev* 65(1):1–43. doi:[10.1128/mmbr.65.1.1-43.2001](https://doi.org/10.1128/mmbr.65.1.1-43.2001)
12. Yip KSP, Stillman TJ, Britton KL, Artymiuk PJ, Baker PJ, Sedelnikova SE, Engel PC, Pasquo A, Chiaraluce R, Consalvi V, Scandurra R, Rice DW (1995) The structure of *Pyrococcus furiosus* glutamate dehydrogenase reveals a key role for ion-pair networks in maintaining enzyme stability at extreme temperatures. *Structure* 3(11):1147–1158. doi:[10.1016/S0969-2126\(01\)00251-9](https://doi.org/10.1016/S0969-2126(01)00251-9)
13. Zhang W, Mullaney EJ, Lei XG (2007) Adopting selected hydrogen bonding and ionic interactions from *Aspergillus fumigatus* phytase structure improves the thermostability of *Aspergillus niger* PhyA phytase. *Appl Environ Microbiol* 73(9):3069–3076. doi:[10.1128/aem.02970-06](https://doi.org/10.1128/aem.02970-06)

14. Liu HL, Wang WC (2003) Protein engineering to improve the thermostability of glucoamylase from *Aspergillus awamori* based on molecular dynamics simulations. *Protein Eng Des Sel* 16(1):19–25
15. Fei B, Cao Y, Xu H, Li X, Song T, Fei Z, Qiao D, Cao Y (2013) AppA C-terminal plays an important role in its thermostability in *Escherichia coli*. *Curr Microbiol* 66(4):374–378. doi:[10.1007/s00284-012-0283-4](https://doi.org/10.1007/s00284-012-0283-4)
16. Kim M-S, Weaver J, Lei X (2008) Assembly of mutations for improving thermostability of *Escherichia coli* AppA2 phytase. *Appl Microbiol Biotechnol* 79(5):751–758. doi:[10.1007/s00253-008-1478-2](https://doi.org/10.1007/s00253-008-1478-2)
17. Pasamontes L, Haiker M, Wyss M, Tessier M, van Loon AP (1997) Gene cloning, purification, and characterization of a heat-stable phytase from the fungus *Aspergillus fumigatus*. *Appl Environ Microbiol* 63(5):1696–1700
18. Noorbatcha IA, Sultan AM, Salleh HM, Amid A (2013) Understanding thermostability factors of *Aspergillus niger* PhyA phytase: a molecular dynamics study. *Protein J* 32(4):309–316
19. Chen Z, Yi Fu Wenbo X, Li M (2013) Molecular dynamics simulation of barnase: contribution of noncovalent intramolecular interaction to thermostability. *Math Probl Eng* 504183
20. Lehmann M, Kostrewa D, Wyss M, Brugger R, D'Arcy A, Pasamontes L, van Loon AP (2000) From DNA sequence to improved functionality: using protein sequence comparisons to rapidly design a thermostable consensus phytase. *Protein Eng Des Sel* 13(1):49–57
21. Lehmann M, Loch C, Middendorf A, Studer D, Lassen SF, Pasamontes L, van Loon AP, Wyss M (2002) The consensus concept for thermostability engineering of proteins: further proof of concept. *Protein Eng Des Sel* 15(5):403–411
22. Lehmann M, Lopez-Ulibarri R, Loch C, Viarouge C, Wyss M, van Loon AP (2000) Exchanging the active site between phytases for altering the functional properties of the enzyme. *Protein Sci* 9(10): 1866–1872. doi:[10.1110/ps.9.10.1866](https://doi.org/10.1110/ps.9.10.1866)
23. Kim MS, Lei XG (2008) Enhancing thermostability of *Escherichia coli* phytase AppA2 by error-prone PCR. *Appl Microbiol Biotechnol* 79(1):69–75. doi:[10.1007/s00253-008-1412-7](https://doi.org/10.1007/s00253-008-1412-7)
24. Zhang W, Lei XG (2008) Cumulative improvements of thermostability and pH-activity profile of *Aspergillus niger* PhyA phytase by site-directed mutagenesis. *Appl Microbiol Biotechnol* 77(5):1033–1040. doi:[10.1007/s00253-007-1239-7](https://doi.org/10.1007/s00253-007-1239-7)
25. Vemparala S, Mehrotra S, Balaran H (2011) Role of loop dynamics in thermal stability of mesophilic and thermophilic adenylosuccinate synthetase: a molecular dynamics and normal mode analysis study. *BBA Protein Proteomics* 1814(5):630–637. doi:[10.1016/j.bbapap.2011.03.012](https://doi.org/10.1016/j.bbapap.2011.03.012)
26. Bae E, Phillips GN (2005) Identifying and engineering ion pairs in adenylate kinases insights from molecular dynamics simulations of thermophilic and mesophilic homologues. *J Biol Chem* 280(35): 30943–30948
27. Pikkemaat MG, Linssen AB, Berendsen HJ, Janssen DB (2002) Molecular dynamics simulations as a tool for improving protein stability. *Protein Eng Des Sel* 15(3):185–192
28. Purmonen M, Valjakka J, Takkinnen K, Laitinen T, Rouvinen J (2007) Molecular dynamics studies on the thermostability of family 11 xylanases. *Protein Eng Des Sel* 20(11):551–559
29. Merlino A, Graziano G, Mazzarella L (2004) Structural and dynamic effects of alpha-helix deletion in Sso7d: implications for protein thermal stability. *Proteins* 57(4):692–701
30. Wintrode PL, Zhang D, Vaidehi N, Arnold FH, Goddard WA III (2003) Protein dynamics in a family of laboratory evolved thermophilic enzymes. *J Mol Biol* 327(3):745–757
31. Meharennia YT, Poulos TL (2010) Using molecular dynamics to probe the structural basis for enhanced stability in thermal stable cytochromes P450. *Biochemistry* 49(31):6680–6686
32. Ding Y, Cai Y (2013) Conformational dynamics of xylanase a from *Streptomyces lividans*: implications for TIM-barrel enzyme thermostability. *Biopolymers* 99(9):594–604
33. de Bakker PI, HuÈnenberger PH, McCammon JA (1999) Molecular dynamics simulations of the hyperthermophilic protein sac7d from *Sulfolobus acidocaldarius*: contribution of salt bridges to thermostability. *J Mol Biol* 285(4):1811–1830
34. Missimer JH, Steinmetz MO, Baron R, Winkler FK, Kammerer RA, Daura X, Van Gunsteren WF (2007) Configurational entropy elucidates the role of salt-bridge networks in protein thermostability. *Protein Sci* 16(7):1349–1359
35. Oh B-C, Choi W-C, Park S, Kim Y-O, Oh T-K (2004) Biochemical properties and substrate specificities of alkaline and histidine acid phytases. *Appl Microbiol Biotechnol* 63(4):362–372
36. Sali A, Blundell TL (1993) Comparative protein modelling by satisfaction of spatial restraints. *J Mol Biol* 234(3):779–815. doi:[10.1006/jmbi.1993.1626](https://doi.org/10.1006/jmbi.1993.1626)
37. Jorgensen WL, Chandrasekhar J, Madura JD, Impey RW, Klein ML (1983) Comparison of simple potential functions for simulating liquid water. *J Chem Phys* 79(2):926–935
38. Hess B, Kutzner C, Van Der Spoel D, Lindahl E (2008) GROMACS 4: algorithms for highly efficient, load-balanced, and scalable molecular simulation. *J Chem Theory Comput* 4(3):435–447
39. Lindorff-Larsen K, Piana S, Palmo K, Maragakis P, Klepeis JL, Dror RO, Shaw DE (2010) Improved side-chain torsion potentials for the Amber ff99SB protein force field. *Proteins* 78(8):1950–1958. doi:[10.1002/prot.22711](https://doi.org/10.1002/prot.22711)
40. Daggett V (2006) Protein folding simulation. *Chem Rev* 106:1898–1916
41. Shaw DE, Maragakis P, Lindorff-Larsen K, Piana S, Dror RO, Eastwood MP, Bank JA, Jumper JM, Salmon JK, Shan Y, Wriggers W (2010) Atomic-level characterization of the structural dynamics of proteins. *Science* 330:341–346
42. Alonso DO, Alm E, Daggett V (2000) Characterization of the unfolding pathway of the cell-cycle protein p13suc1 by molecular dynamics simulations: implications for domain swapping. *Structure* 8:101–110
43. Day R, Bennion BJ, Ham S, Daggett V (2002) Increasing temperature accelerates protein unfolding without changing the pathway of unfolding. *J Mol Biol* 322:189–203
44. Toofanny RD, Daggett V (2012) Understanding protein unfolding from molecular simulations. *WIREs Comput Mol Sci* 2:405–423
45. Badieyan S, Bevan DR, Zhang C (2012) Study and design of stability in GH5 cellulases. *Biotechnol Bioeng* 109:31–44
46. Todde G, Hovmöller S, Laaksonen A, Mocc F (2014) Glucose oxidase from *Penicillium amagasakiense*: characterization of the transition state of its denaturation from molecular dynamics simulations. *Proteins* 82(10):2353–2363
47. Parrinello M, Rahman A (1981) Polymorphic transitions in single crystals: a new molecular dynamics method. *J Appl Phys* 52(12): 7182–7190
48. Cheng A, Merz KM (1996) Application of the Nosé–Hoover chain algorithm to the study of protein dynamics. *J Chem Phys* 100(5): 1927–1937
49. Miyamoto S, Kollman PA (1992) SETTLE: an analytical version of the SHAKE and RATTLE algorithm for rigid water models. *J Comput Chem* 13(8):952–962
50. Hess B, Bekker H, Berendsen HJC, Fraaije JGEM (1997) LINCS: a linear constraint solver for molecular simulations. *J Comput Chem* 18(12):1463–1472. doi:[10.1002/\(SICI\)1096-987X\(199709\)18:12<1463::AID-JCC4>3.0.CO;2-H](https://doi.org/10.1002/(SICI)1096-987X(199709)18:12<1463::AID-JCC4>3.0.CO;2-H)

51. Darden T, Perera L, Li L, Pedersen L (1999) New tricks for modelers from the crystallography toolkit: the particle mesh Ewald algorithm and its use in nucleic acid simulations. *Structure* 7(3):R55–60
52. Humphrey W, Dalke A, Schulten K (1996) VMD: visual molecular dynamics. *J Mol Graph* 14(1):33–38
53. Kabsch W, Sander C (1983) Dictionary of protein secondary structure: pattern recognition of hydrogen-bonded and geometrical features. *Biopolymers* 22(12):2577–2637. doi:[10.1002/bip.360221211](https://doi.org/10.1002/bip.360221211)
54. Thompson MJ, Eisenberg D (1999) Transproteomic evidence of a loop-deletion mechanism for enhancing protein thermostability. *J Mol Biol* 290(2):595–604